

Analysis of surface albedo and
Leaf Area Index from satellite
observations and their impact on
numerical weather prediction

Souhail Boussetta,
Gianpaolo Balsamo, Emanuel Dutra,
Anton Beljaars and Clement Albergel.

Research Department

November 2014

This paper has not been published and should be regarded as an Internal Report from ECMWF.
Permission to quote from it should be obtained from the ECMWF.



Series: ECMWF Technical Memoranda

A full list of ECMWF Publications can be found on our web site under:
<http://www.ecmwf.int/en/research/publications>

Contact: library@ecmwf.int

© Copyright 2014

European Centre for Medium Range Weather Forecasts
Shinfield Park, Reading, Berkshire RG2 9AX, England

Literary and scientific copyrights belong to ECMWF and are reserved in all countries. This publication is not to be reprinted or translated in whole or in part without the written permission of the Director. Appropriate non-commercial use will normally be granted under the condition that reference is made to ECMWF.

The information within this publication is given in good faith and considered to be true, but ECMWF accepts no liability for error, omission and for loss or damage arising from its use.

Abstract

The vegetation state can have a prominent influence on global energy, water and carbon cycles. This has been particularly evident during extreme conditions in recent years (e.g. Europe 2003 and Russia 2010 heat waves, Horn of Africa 2010 drought, and Australia 2010 drought recovery). Weather parameters are sensitive to the vegetation state and particularly to albedo and Leaf Area Index (LAI) that controls the partitioning of the surface energy fluxes into latent and sensible fluxes, and the development of planetary boundary conditions and clouds.

An optimal interpolation analysis of a satellite-based surface albedo and LAI is performed through the combination of satellite observations and derived climatologies, depending on their associated errors. The final analysis products have smoother temporal evolution than the direct observations, which makes them more appropriate for environmental and numerical weather prediction.

The impact of assimilating these near-real-time (NRT) products within the land surface scheme of the European Centre of Medium-Range Weather Forecasts (ECMWF) is evaluated for anomalous years. It is shown that: (i) the assimilation of these products enables detecting/monitoring extreme climate conditions where the LAI anomaly could reach more than 50% and albedo anomaly could reach 10% (in wet years), (ii) extreme NRT LAI anomalies have a strong impact on the surface fluxes, while for the albedo, which has a smaller inter-annual variability, the impact on surface fluxes is small, (iii) neutral to slightly better agreement with in-situ surface soil moisture observations and surface energy and CO₂ fluxes from eddy-covariance towers is obtained, and (iv) in forecast using a land-atmosphere coupled system, the assimilation of NRT LAI reduces the near-surface air temperature and humidity errors both in wet and dry cases, while NRT albedo has a small impact, mainly in wet cases (when albedo anomalies are more noticeable).

1 Introduction

Owing to their influence on the partitioning of energy, mass and momentum fluxes between the land surface and the atmosphere, land surface processes have been shown to substantially impact weather forecasting at short and medium ranges (Koster et al., 2010; Beljaars et al., 1996; Rowell & Blondin, 1990). The impact of land surface processes also extends over different spatial and time scales, and can affect long-term climate projections (Xue et al., 1996; Sellers et al., 1996; Betts et al., 1996; Avissar & Liu, 1996; Boussetta et al., 2008; Balsamo et al., 2009).

As a fundamental component of a land surface model (LSM), the vegetation layer plays a crucial role in the land-atmosphere exchanges. The vegetation contributes to the evaporation through the plant transpiration and direct evaporation of the plant-intercepted precipitation. In addition, it affects the available surface energy through the radiative transfer within the canopy by modifying the surface albedo (Deardorff 1978).

In most LSMs, the Leaf Area Index (LAI), is used as an indicator of the vegetation state (e.g. greening, mature, senescent, dormant). Traditionally, the LAI was represented through look-up tables dependant on the vegetation type (Viterbo & Beljaars, 1995). Although its spatial variation was commonly specified according to the biome types, the temporal variation of the LAI was often neglected and sometimes climatological seasonality was introduced together with other major changes. However, the

impact of the LAI seasonality could not be assessed (Dorman & Sellers, 1989; Giard & Bazile, 2000). With the advent of LAI that is based on satellite observations, the impact of these products within LSMs has been tested at different temporal and spatial scales. By using a satellite-based climatology of LAI within a mesoscale numerical weather prediction (NWP) model, Knote et al. (2009) showed that more realistic LAI information is able to improve the short-range forecast scores of lower-level variables but not their biases. Other studies focused on global circulation models (GCM) and the implications of introducing observed seasonally-varying LAI on the simulations. These studies generally discussed the impact of LAI seasonal (Van den Hurk et al., 2003a; Lawrence & Slingo, 2004) and inter-annual (Guillevic et al., 2002) variability in terms of annual cycle of the hydrological fluxes. They showed that seasonal LAI can have a non-negligible impact on the seasonality of the surface evaporation and precipitation over land. Recently, Boussetta et al. (2013a) introduced a monthly climatology for LAI based on a MODIS satellite product (Myneni et al., 2002) within the European Centre for Medium-Range Weather Forecast (ECMWF) Integrated Forecasting System (IFS) to replace the fixed maximum LAI previously used. They showed that this results in a reduction of near-surface temperature errors in the tropical and mid-latitude areas, especially during spring and summer seasons. However, the direct impact of the use of near-real-time (NRT) LAI observations on surface fluxes and screen-level variables was not investigated.

In addition, the surface albedo was shown to be one of the important parameters that controls the land surface energy balance and subsequently affects the atmospheric boundary layer through the surface radiative balance (Pielke & Avissar, 1990). Initially, NWP systems relied on surface albedo derived from soil type and vegetation type maps, neglecting its seasonal and inter-annual variabilities. Preuss and Geleyn (1983) showed that introducing a seasonally-varying satellite-based climatology of surface albedo into the ECMWF IFS has a small impact on medium-range forecasts and a potentially larger impact at longer ranges. While at a regional scale, Berbet and Costa (2003) showed that over Amazonia, most of the spatial and seasonal variability in the simulated climate after a tropical deforestation can be explained by the variability in surface albedo. These previous studies trigger the question about whether the use of NRT surface albedo has a significant impact on the near-surface atmosphere in comparison to climatological data.

Recently, the Copernicus Global Land products (GEOV1) of surface albedo and LAI based on observations from the VEGETATION sensor on board SPOT satellite (Baret et al., 2007; Verger et al., 2011) have become available in NRT with a foreseen operationally-maintained chain. However, the direct use of these products within a NWP system is not possible without quality checks given the spatial and temporal discontinuities they may contain.

In this study, we explore the assimilation of NRT LAI and surface albedo products in a NWP system using optimal interpolation analysis. We evaluate the impact of the NRT analysis products on surface

fluxes and surface soil moisture derived from land-only offline simulations of the ECMWF land surface model CHTESSEL (Viterbo & Beljaars, 1995; Viterbo et al., 1999; Van den Hurk & Viterbo, 2003b; Balsamo et al., 2009; Dutra et al., 2010; Boussetta et al., 2013a; Balsamo et al., 2011; Boussetta et al., 2013b). The evaluation is then extended to the near-surface air temperature and humidity derived from coupled land–atmosphere simulations using the fully-coupled IFS.

2 The analysis procedure

2.1 The Copernicus global-land products (GEOV1)

The GEOV1 LAI and albedo products are based on observations from the VEGETATION sensor on board SPOT satellite. They are produced every 10 days using a composite observation from a 30 days moving window at $1/112^\circ$ spatial resolution (about 1 km at the Equator) with a global coverage. Each GEOV1 product is provided with its associated error measure σ_0 . To take advantage of previous algorithmic experience and existing LAI products, the “best-performing” LAI data (Garrigues et al., 2008) were combined and then used to train a neural network system (Verger et al., 2011). The combined LAI data are the CYCLOPES-V3.1 (Baret et al., 2007) and the collection 5 of MODIS LAI (Myneni et al., 2002). This fusion benefits from the good performance of MODIS LAI for high values and CYCLOPES-V3.1 LAI at low values. After being trained with the fused data, the neural network system is then fed with the atmospherically-corrected reflectances in red, near-infrared, and shortwave-infrared bands from VEGETATION as well as the solar zenith angles and the satellite overpass timing which results into the GEOV1 LAI (Baret et al., 2013).

The GEOV1 surface albedo is also based on observations from the VEGETATION sensor and its derivation follows Geiger and Samain (2004). The method includes cloud screening (Hagolle et al., 2004), atmospheric correction (Rahman & Dedieu, 1994), directional reflectance normalization (Roujean et al., 1992), and albedo determination for the different integration angles (direct and diffuse) and spectral intervals (visible, near-infrared, and broadband).

Under the Copernicus Global Land framework, the GEOV1 products were validated by analysing their spatial and temporal continuity and consistency as well as their accuracy at the global and regional scales against other global products and the BELMANIP2 sites network (Benchmark Land Multi-site Analysis and Inter-comparison of Products). The conclusion of this validation was that the GEOV1 products are of good quality, show consistent temporal and spatial distributions, and have reasonable accuracy which can meet the requirements for use within LSMs (Camacho et al., 2013).

2.2 Derivation of Climatological series

Before processing the climatological product, unreliable retrievals have been discarded from the analysis using the quality flag (QA). In particular: dead detectors, significant clouds and/or snow

contaminated pixels, and failure of the radiative transfer model due to problems other than geometry have been filtered out during this pre-processing. Afterwards, the 1-km products were aggregated to 10-km resolution through a nine-by-nine-point spatial smoothing. The 10-km value is computed when more than 30% of the 1-km products at the grid point scale have not been flagged and a further snow-free screening is performed on the data. Then a first version of the climatological time series is obtained by averaging data from 1999 to 2012 ($ALB_{c,v1}/LAI_{c,v1}$).

The first version of the climatological time-series still contains gaps, especially in snow-covered high latitude regions. To overcome this deficiency, a second version of the climatological time series ($ALB_{c,v2}/LAI_{c,v2}$) is generated by spatially filling the data gaps with values from 36 10-daily “self-derived” look-up tables of LAI and albedos for each vegetation type. The look-up tables are derived through stratification of $ALB_{c,v1}/LAI_{c,v1}$ by vegetation type based on a 90% vegetation cover threshold for each type. In CHTESSEL, the land use classification follows from the Global Land Cover Characteristics (GLCC) data (Loveland et al., 2000) and use is made of the Biosphere-Atmosphere Transfer Scheme (BATS) classification to assign the vegetation types.

Finally, a three-point temporal smoothing is applied to this second version climatological data to obtain a final version (ALB_c/LAI_c). These data are then re-projected and interpolated to a target model simulation grid, together with their associated error σ_c in order to be used in the ECMWF model. In this study the target model is run at T511 reduced Gaussian grid horizontal resolution which is about 40x40 km.

2.3 Assimilation method

The main objective of data assimilation is to optimize the use of observational data to get the best estimate from all available information. It usually attempts to combine data from different sources in an optimal way to provide the best estimate known as the analysis product. In this study a simple one-dimensional data assimilation method is used to produce analysis of albedo and LAI from the GEOV1 data. Following the method of Gu et al. (2006), two pieces of information are used to generate the analysis product at a given time t : the observation V_o with its associated error σ_o and the climatological values V_c with their associated errors σ_c (V being the LAI or the albedo data). The optimal combination of these two pieces of information is obtained by minimizing a quadratic cost function J which corresponds to the least-square estimate V_a :

$$J(V_a) = \left[\frac{V_a - V_o}{\sigma_o} \right]^2 + \left[\frac{V_a - V_c}{\sigma_c} \right]^2 \quad (1)$$

Assuming the associated errors are Gaussian, the minimisation of J would lead to the BLUE (best linear unbiased estimate) ensuring a minimum variance for the analysis error, which leads to:

$$V_a = \left[\frac{\sigma_c^2}{\sigma_o^2 + \sigma_c^2} \right] V_o + \left[\frac{\sigma_o^2}{\sigma_o^2 + \sigma_c^2} \right] V_c \quad (2)$$

To avoid a rough replacement with the climatological data in the case of missing observation and relax non-realistic jumps, a further processing is performed by adding the climatological tendency to the last analysis value assuming the analysis tendency is similar to the climatological one:

$$\frac{V_a(t) - V_a(t-1)}{\Delta t} = \frac{V_c(t) - V_c(t-1)}{\Delta t} \quad (3)$$

To summarize, a flowchart of the data processing and analysis procedure is illustrated in Figure 1.

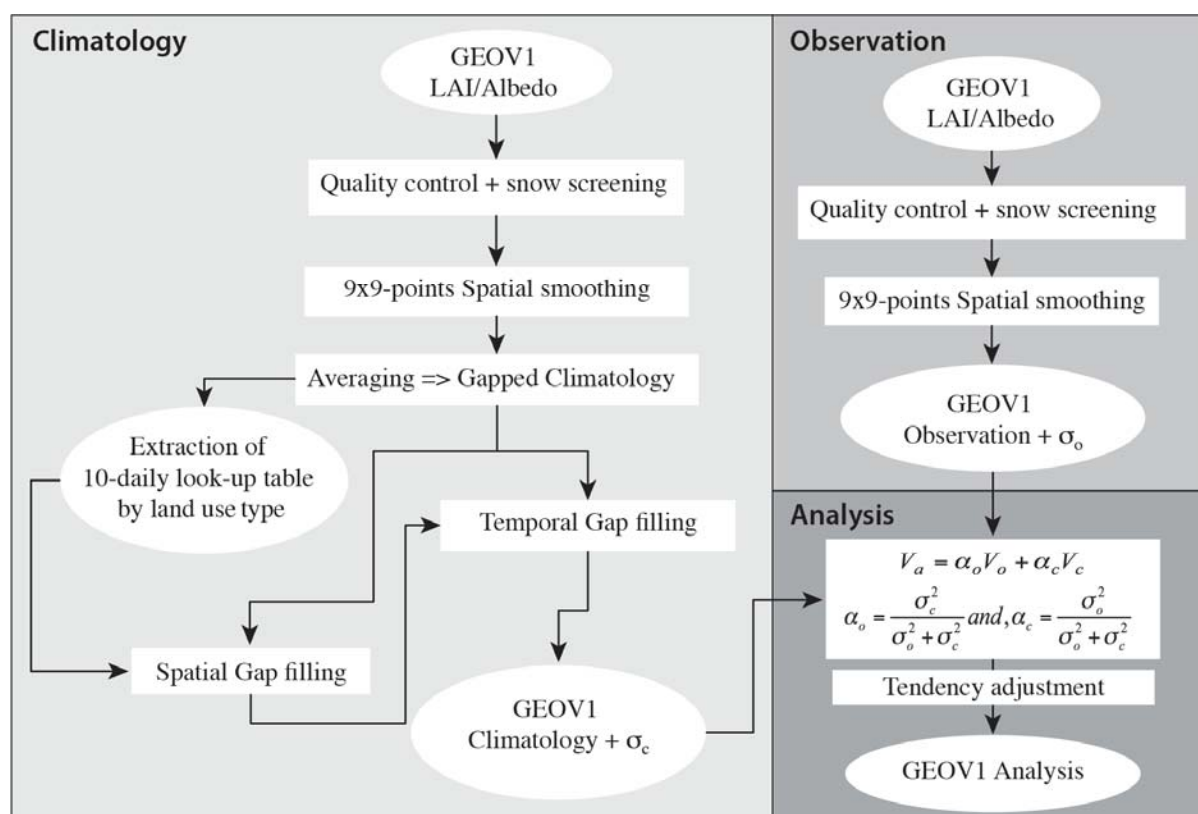


Figure 1: Flowchart of the GEOV1 albedo and LAI pre-processing, climatology derivation and assimilation.

2.4 Characterisation of the analysis products

Using the above-described system, GEOV1 LAI and albedo are assimilated over the 1999–2012 period. Figure 2 presents maps of the analysed LAI and their differences from the observation for dates representative of the four seasons of year 2006 (25 January, 25 April, 25 July and 25 October). The analysis product shows a realistic seasonal evolution and a smooth spatial distribution generally consistent with the vegetation types (Figure 2e, f, g and h). The main spatial features of the LAI on a global scale generally agree with other standard products (as in Fang et al., 2012 and 2013). The

signatures of the African tropical forest, the Amazon area and the European and American Boreal forest, as well as the signature of crop areas like in central Europe and western USA, are correctly captured. Nevertheless, the magnitude and the spatial extent of these signatures can vary significantly depending on regions and seasons. The crops and grass regions show pronounced seasonal cycles with LAI varying between 0.2 and 2.7 [$\text{m}^2 \text{m}^{-2}$], while the boreal forest shows smaller seasonal amplitude for the evergreen needle-leaf from 1.2 to 4.2 [$\text{m}^2 \text{m}^{-2}$] and higher variation from 0.8 to 4.0 [$\text{m}^2 \text{m}^{-2}$] for the deciduous needle-leaf. The tropical forests have a very mild seasonal cycle with an average amplitude of 0.3 [$\text{m}^2 \text{m}^{-2}$].

The differences with the observation data show that the assimilation is most active in high latitudes where the original products are most affected by snow. This is particularly visible in winter, spring and late autumn (Figure 2a, b, d). On the other hand, the summer season shows the least differences, especially in high latitudes where problems from snow contamination are minimal (Figure 2c). Also in the tropical regions the difference with the assimilated LAI suggests a higher weight of the climatology mainly caused by the cloud contamination of the observed data. At the high latitudes ($> 70^\circ\text{N}$), the positive correction in the Siberian tundra with a smooth transition toward the other regions shows the effectiveness of the extracted look-up tables in filling gaps, even in region with no observations (Figure 2c). This suggests that the analysed LAI has indeed benefited from the processing chain and led to a superior data usable for environmental applications.

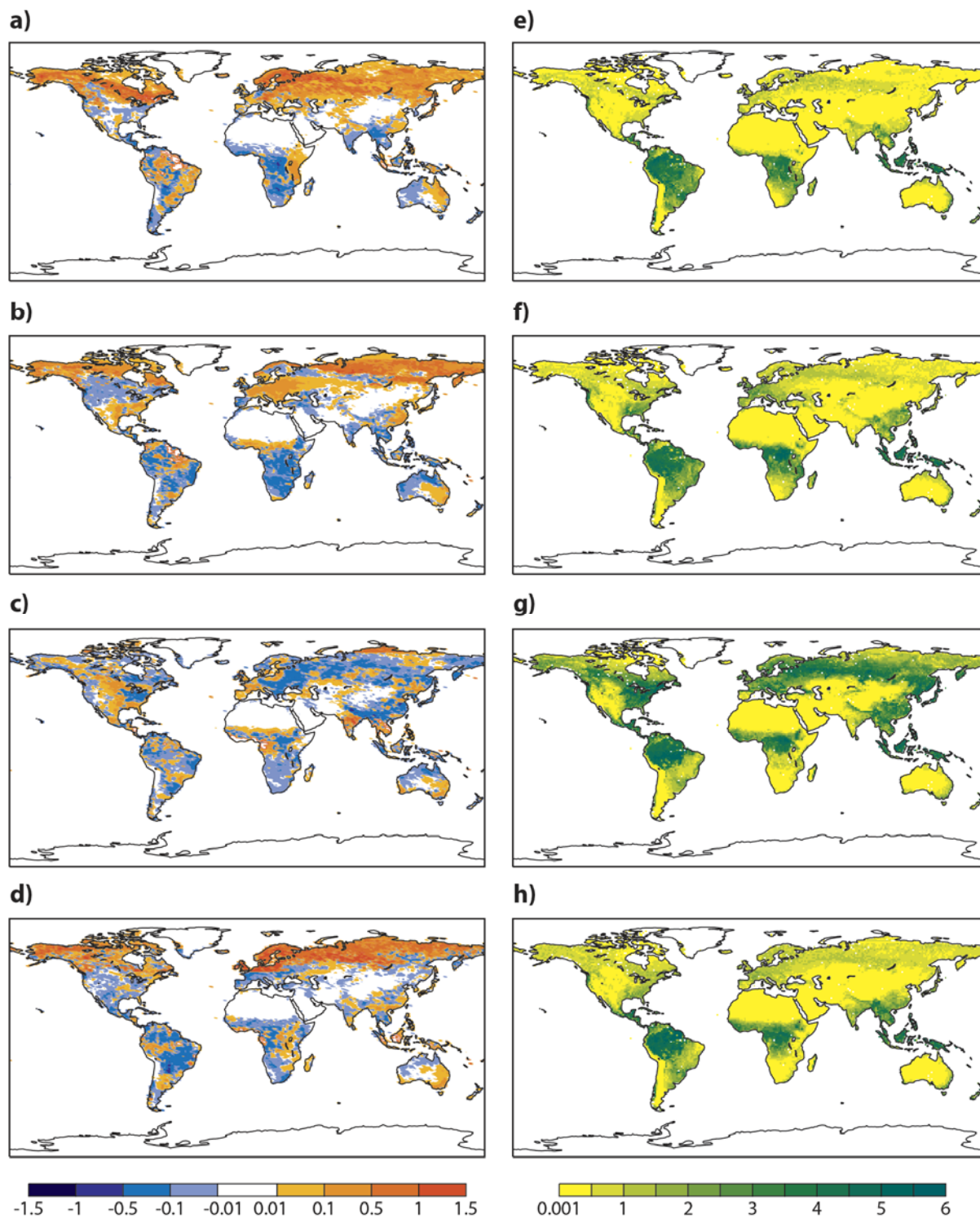


Figure 2: Differences between the analysed LAI and the observed LAI [$m^2 m^{-2}$] for a) 25 January 2006, b) 25 April 2006, c) 25 July 2006, and d) 25 October 2006, and the analysed LAI [$m^2 m^{-2}$] for e) 25 January 2006, f) 25 April 2006, g) 25 July 2006, and h) 25 October 2006.

Considering the albedo product, similarly to Figure 2, Figure 3 shows the analysis of snow-free broadband diffuse albedo and its difference from the observed data for dates representing the four

season of year 2006 (25 January, 25 April 25, 25 July and 25 October). As expected from such data, the desert areas show very small seasonal and spatial variations, while the other regions show a spatial distribution similar to the MODIS data (Gao et al., 2005). In terms of seasonal variation, the analysis product shows a consistent response to vegetation that is seasonality associated with the background bare soil exposure (Figure 3e, f, g and h). The European boreal forest, for instance, displays a consistent albedo evolution related to the forest growth seasonality. Similarly, the deciduous broadleaf forest albedo in the southern area of the tropics displays an evolution consistent with the LAI analysis maps (Figure 2). The signal from low vegetation regions shows a less obvious pattern as the background bare soil can play a stronger compensating role in the albedo value. However, these types generally display an increase of the albedo toward the summer, especially over grass and crop areas; even when the soil background is more exposed, it displays a brighter albedo linked to a soil moisture decrease.

Figure 3a, b, c and d shows that in general the differences between the analysed and the observed albedo are more homogeneous than the LAI ones: this is mainly due to the small variability of the broadband albedo compared to LAI in characterizing the land use. The highest differences are associated with higher observation errors over snow covered areas and a large illumination angle in high latitudes. This is particularly seen in spring and winter when the assimilation procedure has the highest impact. The lowest adjustment occurs in the summer months (Figure 3c) when snow is absent. However, the analysed albedo tends to have higher differences with that observed in cloud contaminated area as it is the case for the Indian peninsula and the West-African monsoon region.

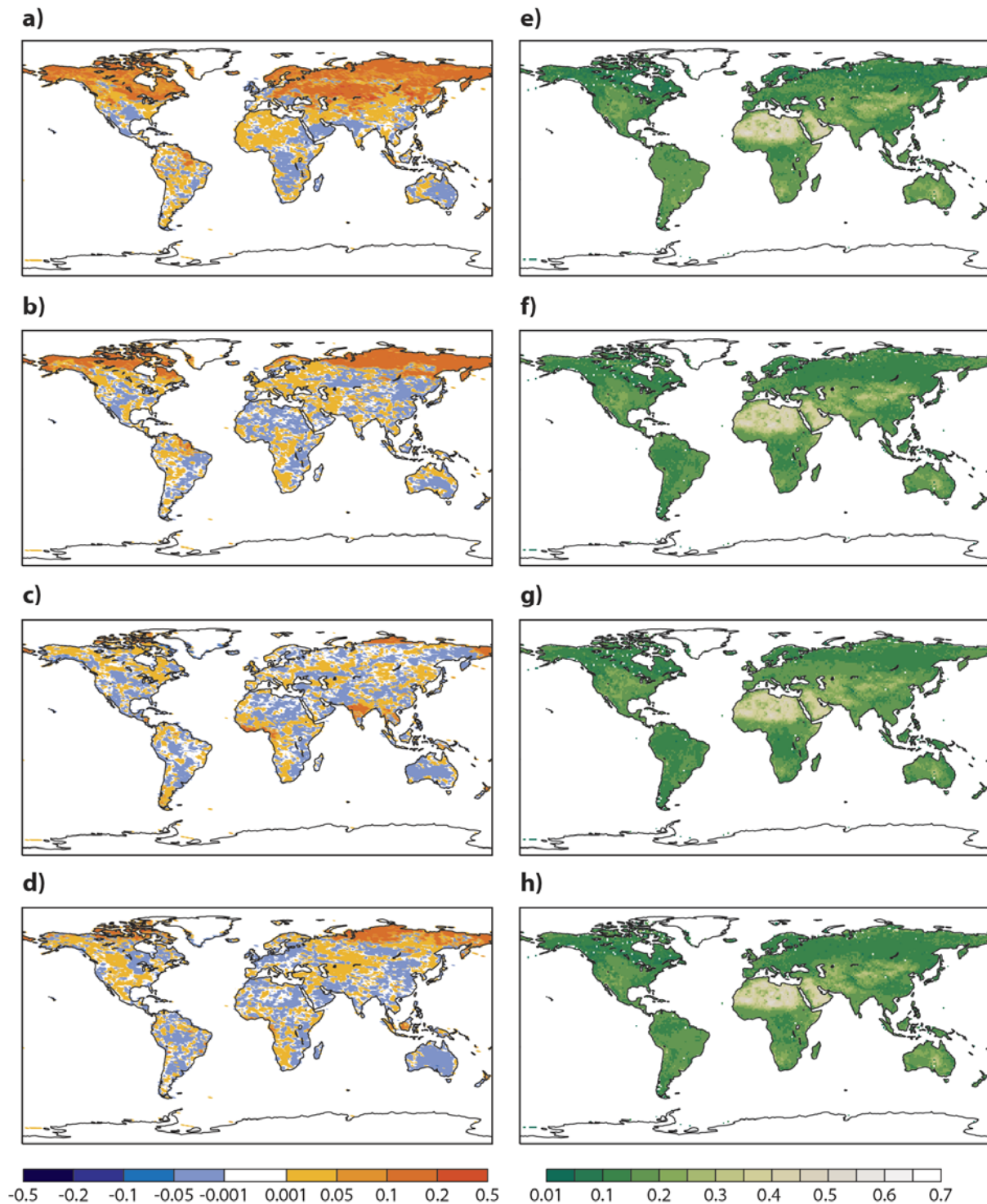


Figure 3: Differences between the analysed and the observed broadband diffuse albedo for a) 25 January 2006, b) 25 April 2006, c) 25 July 2006, d) 25 October 2006, and analysed broad band diffuse albedo for e) 25 January 2006, f) 25 April 2006, g) 25 July 2006, and h) 25 October 2006.

2.5 Inter-annual variability and anomalies in the analysis products

Given that the focus of this study is also to check the impact of the assimilated NRT products on the surface fluxes and the near-surface atmospheric variables, a pre-assessment of the difference between the NRT analysis products and their respective own climatologies is necessary. For the sake of completeness and to be able to only extract the NRT effect, new 10-daily climatological data are generated by averaging the analysis products through the whole 1999–2012 period. In the remainder of this paper, reference to climatology is associated to this new product. Figure 4 displays the relative anomaly $\left(\frac{100*(NRT - CLIM)}{CLIM}\right)$ of the analysed LAI (left panel) and analysed albedo (right panel) with regard to their 1999–2012 climatologies for three known extreme event cases: the 2003 European drought (upper panel), the 2010 Russian summer heat wave (middle panel) and the 2010 Horn of Africa drought which occurred at the same period as a drought recovery in Australia (lower panel). Figure 4 shows that for these cases, the LAI anomaly is generally more pronounced than the albedo anomaly. The LAI anomaly can reach 80% of the climatological values, whereas the albedo anomaly does not exceed 20%. In addition, the albedo anomaly is more pronounced in extreme wet cases such as in central Australia during the wet period of November 2010 where the anomaly reached -10%, while LAI anomaly is perceptible in both dry and wet cases (e.g. the anomaly during the Horn of Africa drought reached -40% and the anomaly over the central Australia attained +40% of the climatological values). Owing to the soil background exposure compensation which also depends on the soil type and moisture, the link between LAI anomaly and albedo anomaly is not always clear. However Figure 4 shows that a positive LAI anomaly is generally associated with a negative albedo anomaly in low vegetation areas. 20% to 40% LAI positive anomaly correspond to a 1% to 10% negative albedo anomaly depending on the low vegetation type and cover.

The inter-annual variation of the analysis LAI and albedo is depicted in Figure 5 by time series over the regions where extreme events occurred in 2010 (central Australia and Horn of Africa and Russia). The variability over Russia is smaller than that of the Horn of Africa or central Australia. This suggests that the inter-annual variability of LAI and albedo are more pronounced over regions with low vegetation, which could be explained by the impact of the tighter link between the underlying soil moisture and low vegetation growth in comparison with the high vegetation one, as well as the relation with the background soil exposure and cover. In addition, in term of absolute value, the inter-annual variability of LAI is larger than the variability of albedo. For instance, over the Horn of Africa the difference between the LAI of November 2006 and November 2010 is more than 100%. It is also the case between October 2002 and October 2010 over central Australia. However the albedo variability does not exceed 10% over those regions.

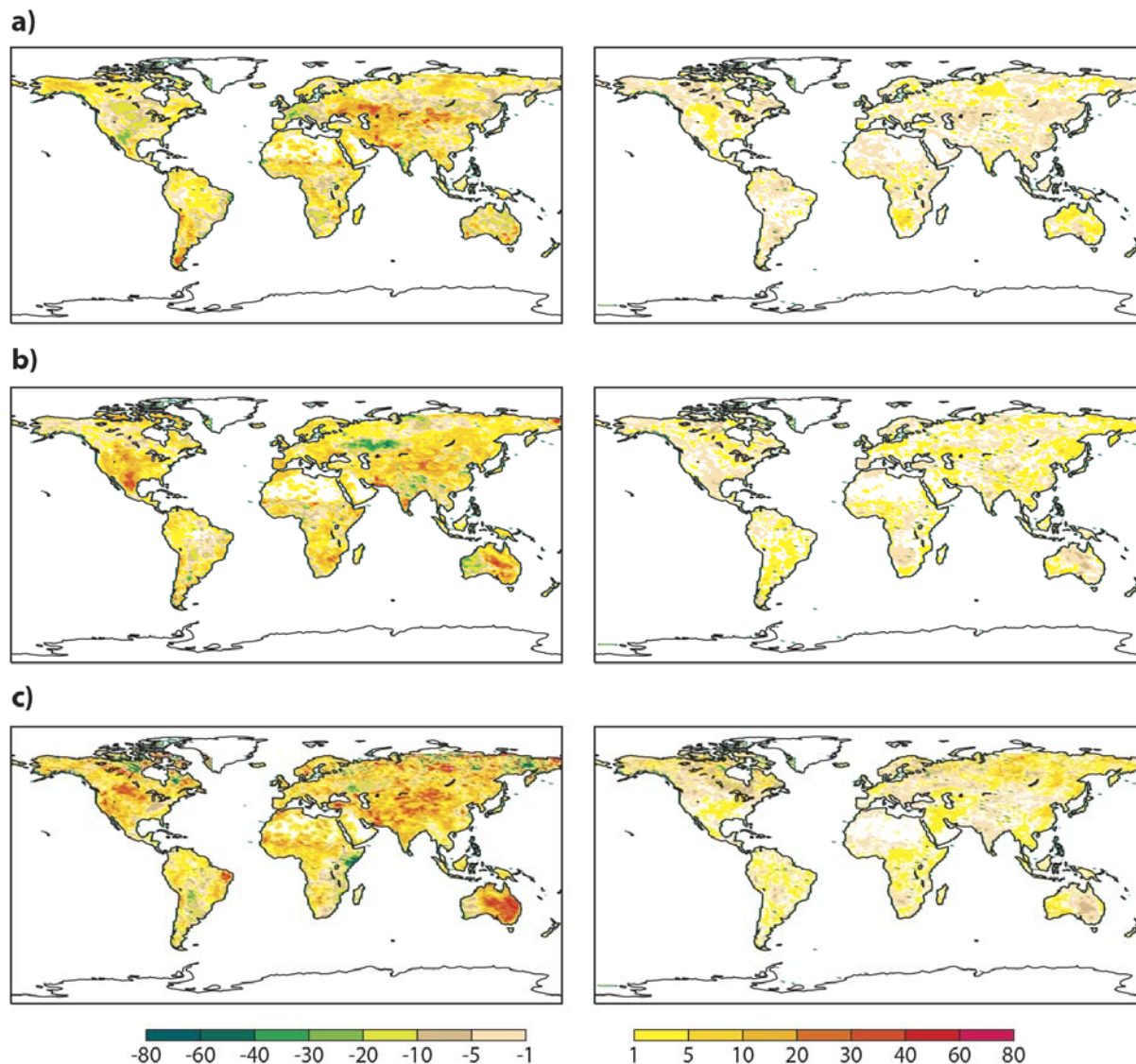


Figure 4: Relative anomaly [%] of LAI (left) and broadband diffuse albedo (right) for a) August 2003, b) July 2010 and c) November 2010.

Focusing on the 2010 extremes events, during the July 2010 Russian heat waves, the LAI was lower than the 10th percentile of the whole 1999–2012 period, while the albedo was between the 70th and 90th percentile. In the case of the Horn of Africa drought (November 2010), the LAI was much lower than the 10th percentile whereas the albedo was higher than the 90th percentile. While in the case of the drought recovery over Australia during the same period, the LAI of central Australia was at its maximum and much higher than the 90th percentile and the albedo reached its 10th percentile. This almost direct opposite relation between LAI and albedo in terms of percentiles is not translated in absolute anomalies because LAI variability is higher than the albedo one.

The above results confirm that with the assimilation system, the GEOV1 NRT LAI and albedo have smoother and more realistic fields that are capable of mimicking their inter-annual variability and

correctly detect and monitor extreme events. Given the important role of LAI and albedo in the radiative forcing and the surface energy and water budgets, it is expected that, compared to the climatological fields, the use of NRT LAI and albedo analysis would have an impact on surface carbon and energy fluxes and subsequently affect the prediction of the near-surface temperature and humidity.

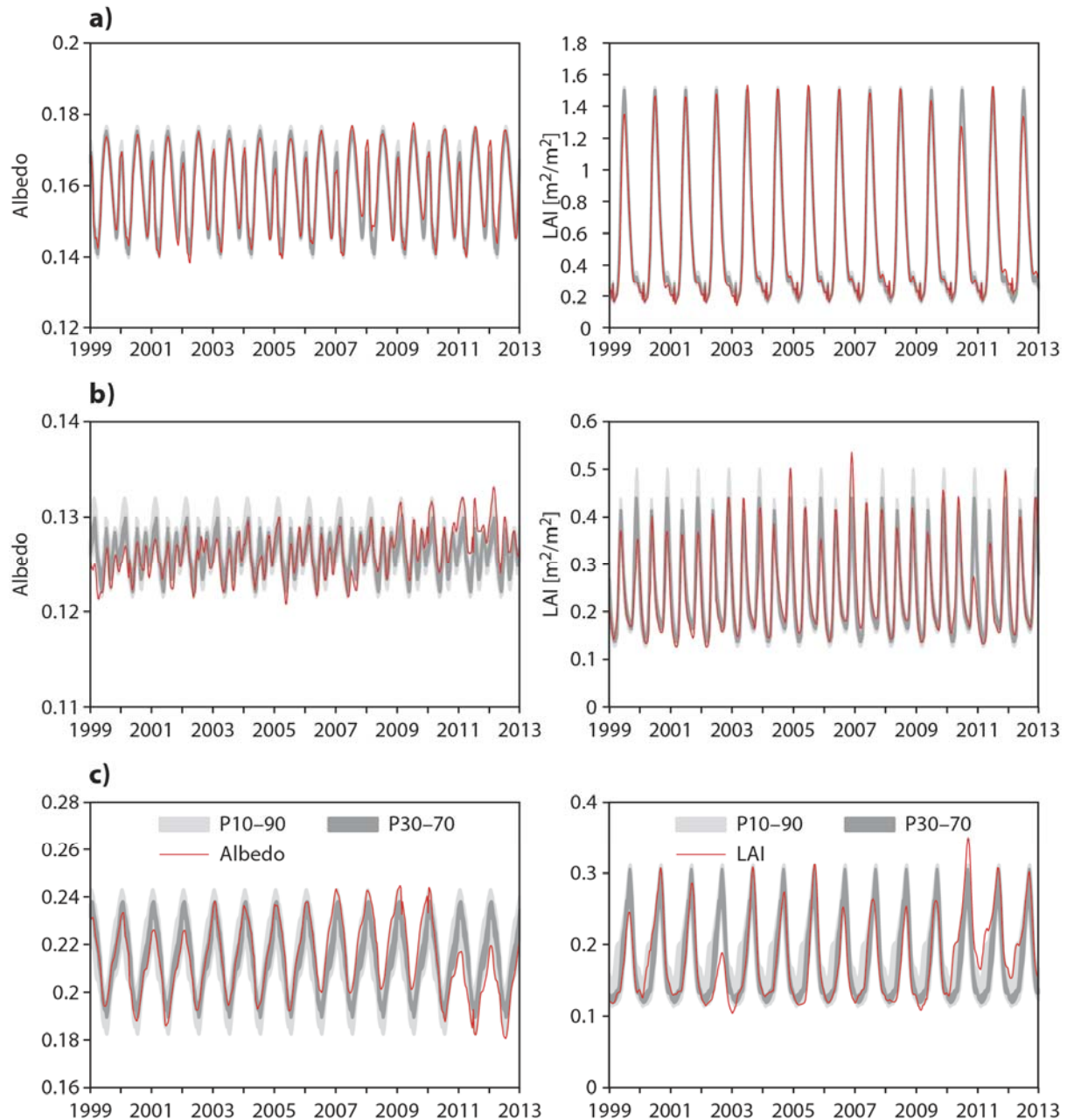


Figure 5: Time series (red) of albedo (left) and LAI (right) for a) Russia, July 2010, b) Horn of Africa and c) central Australia, November 2010. 10–90th percentile (light grey) and 30–70th percentile (dark grey).

3 Impact on the surface-atmosphere interaction within the ECMWF NWP system

In this section, by focusing on the extreme events previously identified, we examine the impact of the assimilation of NRT LAI and albedo on surface fluxes and surface soil moisture derived from CHTESSEL offline simulation as well as on the near-surface air temperature and humidity derived from coupled forecast simulations using the ECMWF IFS. The evaluation is performed by comparing against control simulations based on climatological LAI and albedo. The surface fluxes are also evaluated against available FLUXNET eddy-covariance network (Baldocchi et al., 2001; Baldocchi et al., 2008) and the Boreal Ecosystem Research and Monitoring Sites (BERMS, Betts et al., 2006) data for 2003 as no flux data was available to us in 2010, while the surface soil moisture are evaluated against 2010 data from the International Soil Moisture Network (ISMN, Dorigo et al., 2011; <http://ismn.geo.tuwien.ac.at/>). The evaluation procedure is described in Figure 6.

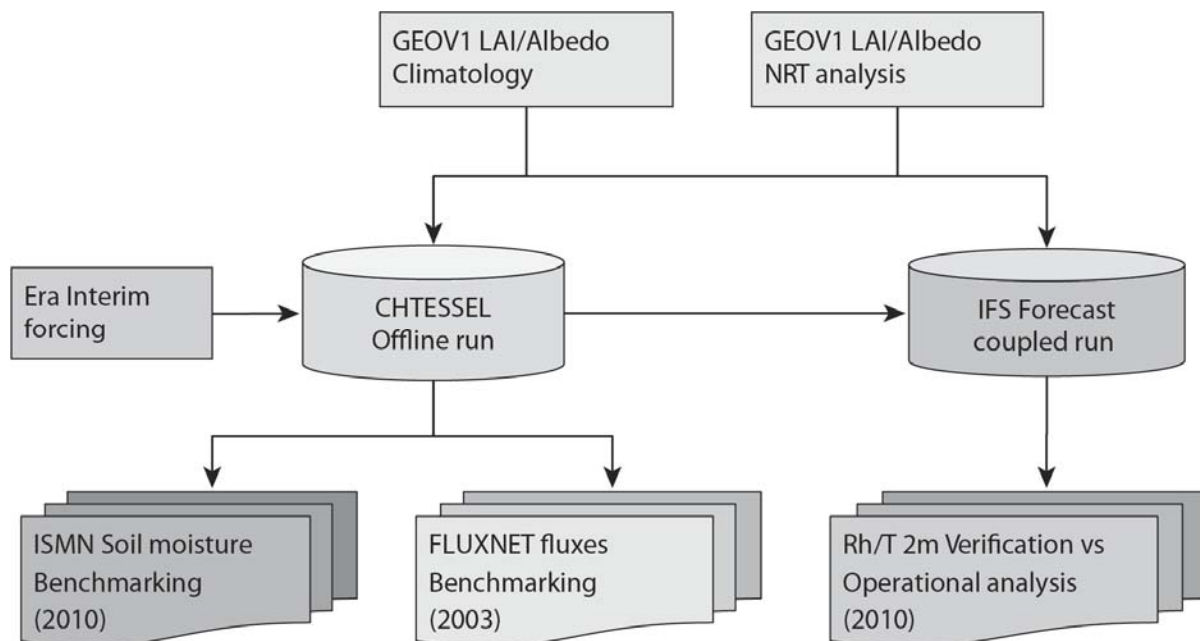


Figure 6: Evaluation procedure of the impact of NRT LAI/albedo analysis.

3.1 Offline simulations

The offline (or stand-alone) simulations offer a computationally-efficient and controlled framework for studying the benefits and deficiencies of a given land surface parameterization without having to consider complex surface/atmosphere interactions as present in a coupled mode.

The offline simulations are performed at the global scale for the period covering the GEOV1 data (1999 to 2012). However, the results are focused on 2010 because it contains contrasting extreme events in the Horn of Africa and Australia as shown in the previous section. All the land simulations

are forced with 3-hourly meteorological data extracted from the ECMWF ERA-Interim (ERA-I) reanalysis (Dee et al., 2011). These forcing data originally produced on a T255 reduced Gaussian grid are spatially interpolated to a T511 grid corresponding to a resolution of about 40 km. The temperature, surface pressure, humidity and wind fields are instantaneous values and representative of the lowest level in the atmospheric model that is at 10 m above the surface. The incoming surface radiation (in its long- and short-wave components), rainfall and snowfall are provided as 3-hourly accumulations. The instantaneous fields are linearly interpolated in time to the 30 minutes time-step of the land surface model. They are from the 3-, 6-, 9- and 12-hour forecasts starting from the daily analyses at 00 and 12 UTC. As a compromise between spin-up effects (mainly in radiation) and forecast errors, the fluxes are averages from the 3-hourly forecast intervals 9–12, 12–15, 15–18 and 18–21 hours starting from the daily analyses at 00 and 12 UTC (see Kallberg (2011) for a discussion on the spin-up characteristics of ERA-I). Fluxes and instantaneous fields are matched by verification time. Precipitation is kept constant over the 3-hourly interval, long-wave downward radiation is linearly interpolated and downward solar radiation is disaggregated in time making use of the solar angle, but conserving the 3-hourly integral. The land-use information is derived from the GLCC data set (Loveland et al., 2000) at the same resolution as the forcing data.

Four global offline model integration experiments are performed:

- i. A control run where the GEOV1 LAI and albedo climatological products are used to force the CHTESSEL model (SCLIM).
- ii. An experiment run where CHTESSEL is constrained using the analysis products of GEOV1 NRT LAI and albedo (SNRT).
- iii. An experiment run where CHTESSEL is constrained using the analysis products of GEOV1 NRT LAI and albedo data is from climatology (SLAINRT).
- iv. An experiment run where CHTESSEL is constrained using the analysis products of GEOV1 NRT albedo and LAI data is from climatology (SALBNRT).

The different experiment configurations are summarized in Table 1.

The comparison between these experiments allows the evaluation of the impact of using the NRT LAI and albedo with reference to the use of climatology. To be able to detect such an impact, focus is mainly on the 2010 known anomalies.

Table 1: Experiments configuration to assess the assimilation of NRT LAI and albedo impact.

EXPERIMENT Type	NAME	LAI	Albedo	Surface initial conditions	PERIOD
Surface offline	SCLIM	Climatology	Climatology	ERA-Interim	1999–2012
Surface offline	SNRT	NRT	NRT	ERA--Interim	1999–2012
Surface offline	SLAINRT	NRT	Climatology	ERA-Interim	1999–2012
Surface offline	SALBNRT	Climatology	NRT	ERA-Interim	1999–2012
Forecast	FCLIM	Climatology	Climatology	SCLIM	2010
Forecast	FNRT	NRT	NRT	SNRT	2010
Forecast	FLAINRT	NRT	Climatology	SLAINRT	2010
Forecast	FALBNRT	Climatology	NRT	SALBNRT	2010

3.1.1 Impact on CO₂ fluxes

Figure 7 shows November 2010 global Net Ecosystem Exchange (NEE) difference between the experiment SNRT where the model is constrained by NRT LAI and albedo, and the control run SCLIM based on the climatological GEOV1 LAI and albedo. November 2010 is characterized by a drought in the Horn of Africa and a wet event corresponding to drought recovery in central and eastern Australia as identified in the previous section (Figures 4 and 5). In the Horn of Africa, the run with climatological data (Figure 7a) shows that in November the region is under a respiration regime¹, and the difference plot shows an anomaly that reaches more than 50%. The difference (anomaly) of the absolute fluxes is shown in Figure 7c, b, d, such that positive indicates an increase and negative indicates a decrease in the flux independent of its direction. These results suggest that the respiration increase is mainly due to the decrease in LAI (Figure 7b, c), as the difference with the simulation using only NRT albedo (SALBNRT) is not significant (Figure 7d). This anomaly is well above the 90th percentile of the whole 14 years period (1999–2012) considered in this study (Figure 8, left) which is consistent with the LAI negative anomaly (Figure 5).

¹ By model convention downward fluxes are positive, so respiration is negative.

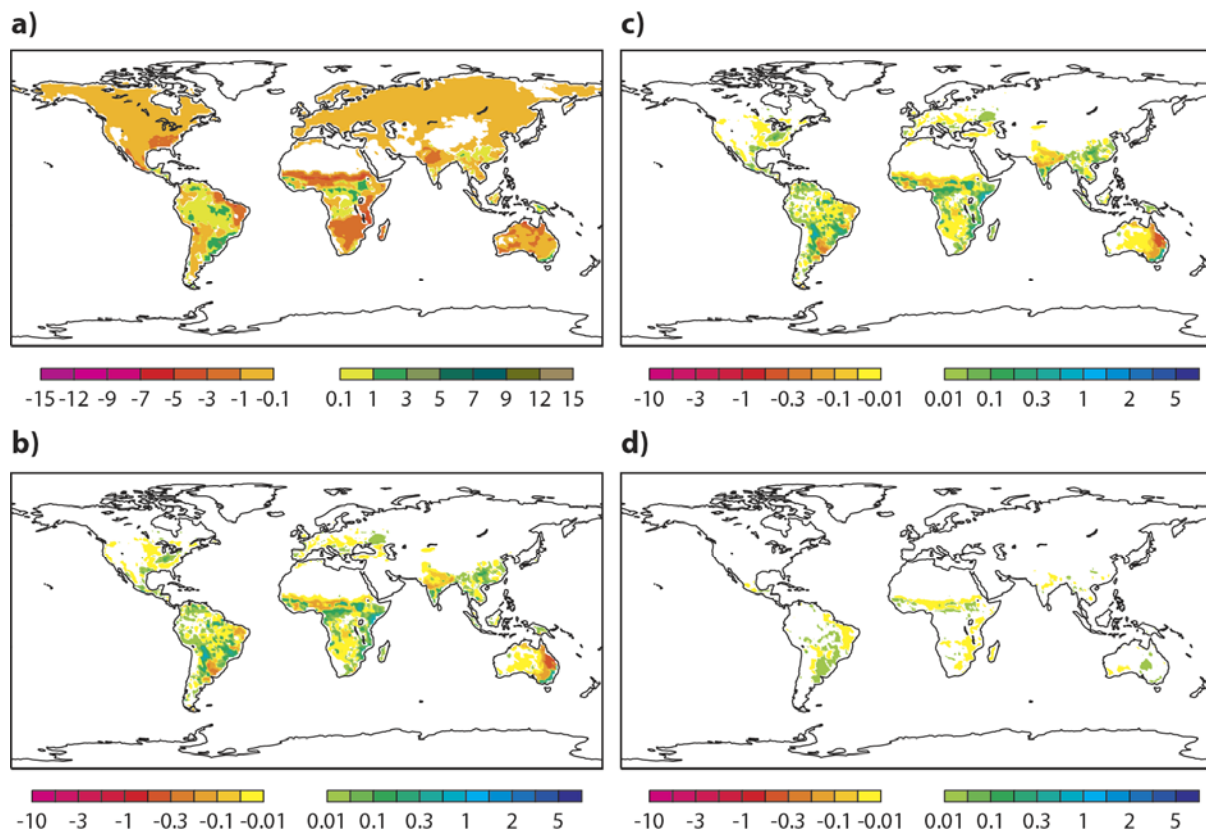


Figure 7: Net Ecosystem exchange [$\mu\text{mol}/\text{m}^2/\text{s}$] for November 2010, a) using GEOVI climatological LAI and albedo (SCLIM). Anomalies are shown as differences with respect to SCLIM for simulations using b) LAI and albedo NRT analysis (SNRT), c) LAI NRT analysis and albedo climatology (SLAINRT) and d) albedo NRT analysis and LAI climatology (SLBNRT).

For the Australia wet case, the results from the SCLIM experiment show an overall respiration regime and a localized photosynthesis regime at the east to southeast region. The difference with the SNRT experiment shows a decrease in respiration and an increase in photosynthesis both explained by the co-located LAI positive anomaly (as seen on Figure 4). The NEE anomaly in this case also reached more than 50%, and the anomaly for the central part of Australia (Figure 8, right) was less than the 10th percentile corresponding to the LAI anomaly which exceeded the 90th percentile for the same region (Figure 5). The NRT albedo analysis impact (SALBNRT experiment) shows a very small increase in the respiration although its anomaly was at the 10th percentile level (Figure 5).

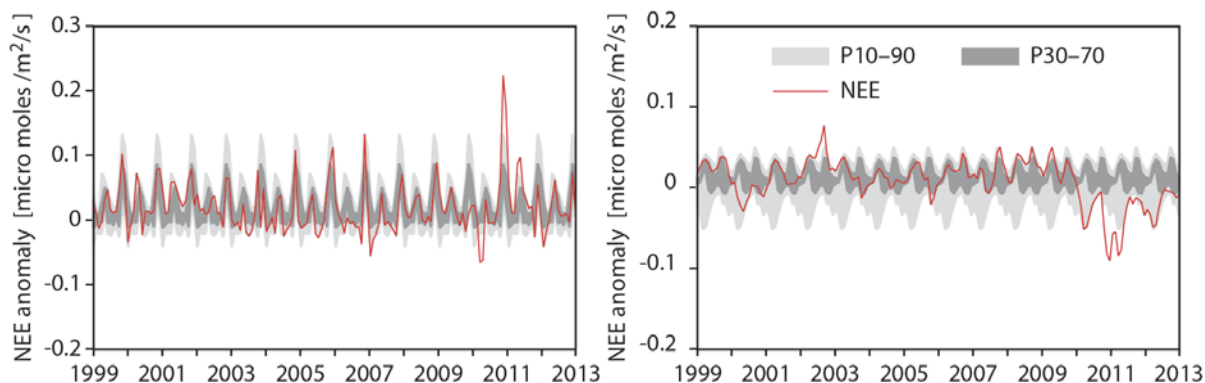


Figure 8: Time series of the Net Ecosystem Exchange [micromoles/m²/s] for the Horn of Africa (left), and for central Australia (right).

3.1.2 Impact on the energy fluxes

Similar to the CO₂ flux, the energy fluxes for November 2010 were also affected by the LAI and albedo anomaly detected in the GEOV1 NRT analysis product. As a consequence to the observed decrease of LAI over the Horn of Africa, a decrease in the Latent heat flux (Figure 9b, c) and an increase in the sensible heat flux (Figure 10b, c) were obtained by the model for both SLAINRT and SNRT configurations. The experiment using only the albedo NRT analysis (SALBNRT) shows a minor decrease in both latent and sensible heat fluxes related to a mild increase of the surface albedo (Figure 5b) which induces a decrease in the net surface radiation. In this case, the increase of the surface albedo is due to the brightening of the surface caused by the drought condition. However, when combined, the NRT LAI and albedo (SNRT), the resultant anomaly signal of both latent (Figure 9b) and sensible heat fluxes (Figure 10b) is mainly driven by the LAI anomaly.

In the case of the wet anomaly over Australia, an opposite behaviour is observed. The LAI positive anomaly in both SNRT and SLAINRT configurations resulted in an increase of the latent heat flux and a decrease of the sensible heat flux, especially over the densely vegetated area in the eastern region. In the central Australia region which is less vegetated, the wet condition led to a decrease of the surface albedo resulting in an increase of the sensible heat flux (SALBNRT and SNRT). This effect was more important than the decrease caused by the LAI anomaly (SLAINRT) due to the small vegetation cover in this region as depicted in (Figure 10).

In summary, this impact of the LAI and albedo anomalies on the energy and carbon fluxes shows the potential of the model when combined with NRT data in simulating and monitoring extremes events.

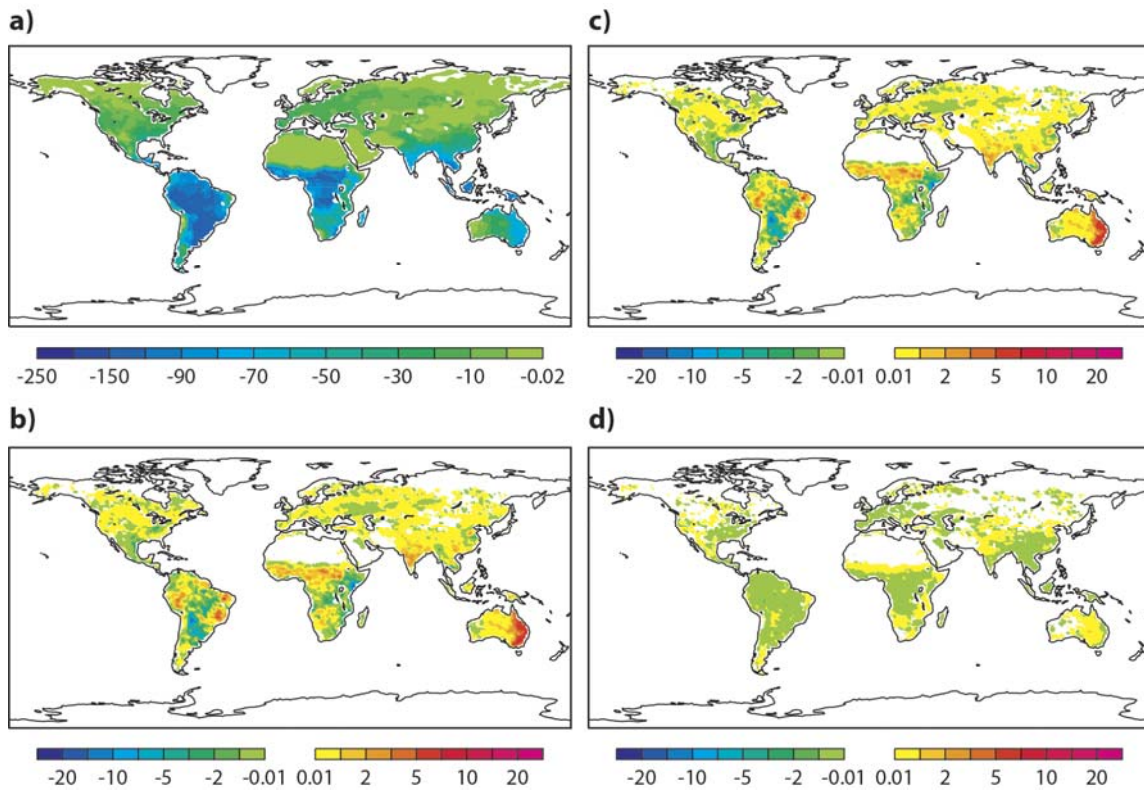


Figure 9: Similar to Figure 7 for the latent heat flux [$W m^{-2}$].

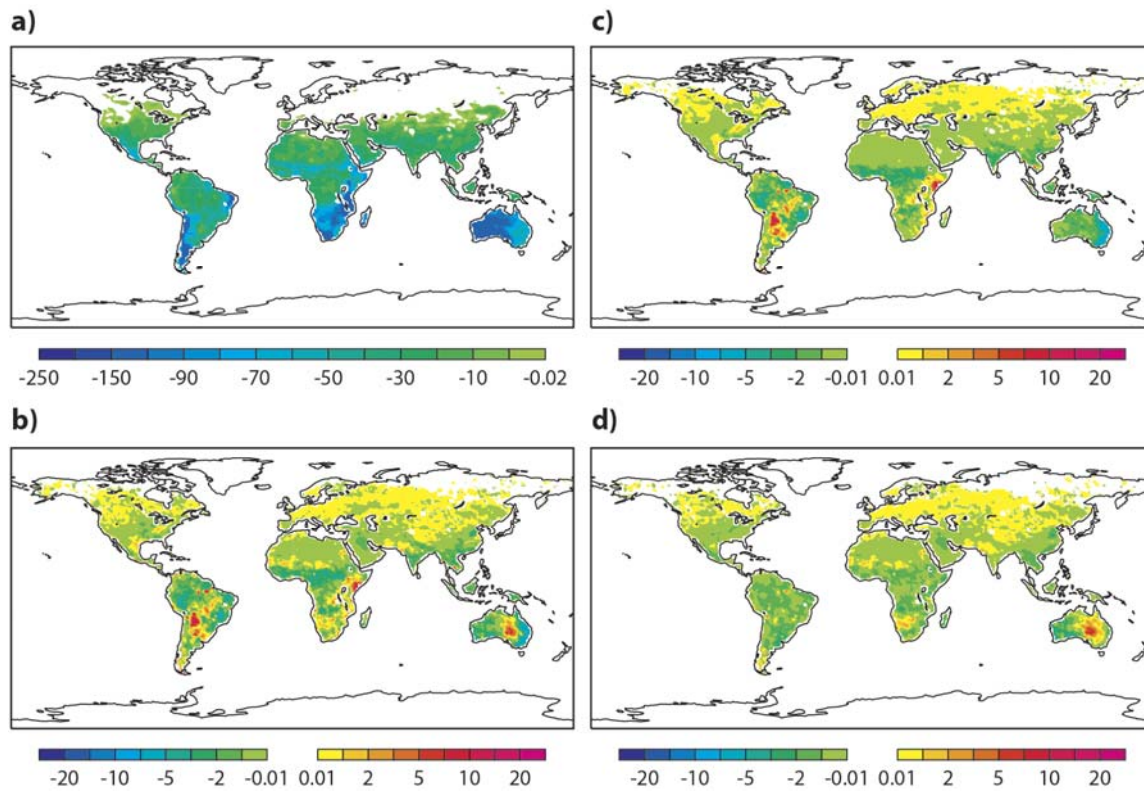


Figure 10: Similar to Figure 7 for the Sensible Heat flux [$W m^{-2}$].

3.1.3 Comparison with in-situ observations

Given the lack of in-situ data over the considered areas for November 2010, an accurate quantitative assessment of the simulated flux differences is not possible. However, a general assessment of the NRT LAI and albedo is performed with the available flux and soil moisture observations using 52 FLUXNET sites in 2003 and 523 sites from the ISMN in 2010. The later belongs to 8 networks located over contrasting biomes and climate conditions.

Table 2 shows the average benchmarking metrics of the model simulations against 52 FLUXNET sites for 2003. In this case, the observation sites were mainly located in Europe and North America. Slightly better agreement with in-situ surface energy and CO₂ fluxes is obtained when NRT data is used, although the magnitude of the improvement is quite small and in some cases may not be within the significance range. For the energy fluxes, the use of the NRT data reduces the latent heat fluxes bias for 69% of the sites used in this comparison. In the case of the sensible heat fluxes, using LAI NRT and albedo NRT reduces the bias for 67% of the sites while when using LAI NRT and albedo climatology the bias is reduced for 75% of the sites. The different simulation results have an equal average correlation over the 52 sites (0.85 for the latent heat flux, 0.74 for the sensible heat flux and 0.82 for the CO₂ flux). However, in terms of the number of sites with improved metrics, the correlation of the gross primary production increased for 57% of the sites when using NRT LAI and albedo and for 63% of the sites when NRT LAI and albedo climatology are used. The comparison between SNRT and SLAINRT related to the use of both NRT LAI and albedo or only LAI NRT respectively suggests that the LAI NRT signal is in general dominant although the albedo NRT tends to reduce the sensible heat flux bias as albedo has a direct impact on this variable.

Table 2: Flux evaluation averaged against 52 FLUXNET sites for 2003: metrics based on 10-day averaged simulated fluxes. The confidence Interval (CI) of RMSE is based on the Chi-squared distribution and the 95% CI of the mean correlation is based on the Fisher Z-transform.

Flux	SCLIM			SLAINRT			SNRT		
	RMSE	Bias	Corr.	RMSE	Bias	Corr.	RMSE	Bias	Corr.
Latent Heat [W/m²] N sites better than SCLIM	20.9 (±0.7)	10.40	0.85 (±0.01)	20.6 (±0.7)	9.60	0.85 (±0.01)	20.6 (±0.7)	9.63	0.85 (±0.01)
	-	-	-	34	36	27	33	36	25
Sensible Heat [W/m²] N sites better than SCLIM	20.3 (±0.7)	-1.64	0.74 (±0.02)	20.4 (±0.7)	-1.77	0.74 (±0.02)	20.5 (±0.7)	-1.26	0.74 (±0.02)
	-	-	-	26	39	28	25	35	29
Gross Primary Prod. [μmole/m ² /s] N sites better than SCLIM	2.06 (±0.07)	0.80	0.81 (±0.01)	2.12 (±0.07)	0.88	0.82 (±0.01)	2.12 (±0.07)	0.88	0.82 (±0.01)
	-	-	-	25	18	33	25	18	31

Similarly for the soil moisture benchmarking (Table 3), the signal of the improvement owing to the assimilation of NRT LAI and albedo is quite small although more than 50% of the modelled sites experienced a minor improvement in their correlation with the observed soil moisture. This signal is equally valid for the surface which is evaluated against 523 sites of the ISMN and for the root-zone for which the evaluation is only performed on 58 sites of the USCRN network (Bell et al., 2013) given the availability of observations.

In addition, it is important to note that the metrics shown represent an average for all the sites considered for a full year. Therefore, the impact of any inter-annual variability or anomaly signal that NRT data may hold in some sites will be diluted with sites having a “climatological” year behaviour. However, at the regional and global scales, an indirect assessment would be feasible by meteorologically evaluating the LAI and albedo NRT analysis impact on near-surface temperature and humidity and precipitation forecasts.

Table 3: Averaged metrics for surface and root-zone soil soil moisture benchmarking against the ISMN sites for 2010 based on daily soil moisture values. The confidence Interval (CI) of RMSE is based on the Chi-squared distribution and the 95% CI of the mean correlation is based on the Fisher Z-transform.

Soil moisture/Exp	SCLIM			SLAINRT			SNRT		
	RMSE	Bias	Corr.	RMSE	Bias	Corr.	RMSE	Bias	Corr.
Surface (523 sites)	0.138	-0.108	0.688	0.137	-0.107	0.690	0.137	-0.107	0.691
	(±0.0004)		(±0.002)	(±0.0004)		(±0.002)	(±0.0004)		(±0.002)
N sites better than SCLIM	-	-	-	297	293	307	307	312	297
Root zone (58 sites)	0.114	-0.064	0.698	0.113	-0.062	0.700	0.113	-0.062	0.700
	(±0.001)		(±0.007)	(±0.001)		(±0.007)	(±0.001)		(±0.007)
N sites better than SCLIM	-	-	-	33	34	32	35	36	30

3.2 Forecast experiments

To evaluate the impact of the assimilation of NRT LAI and albedo on the surface–atmosphere interaction, a series of 3-day forecasts initialised every day from 1 January 2010 00UTC to 31 December 2010 00UTC was performed using the different LAI and albedo products. Given the different time scales between land surface processes and atmosphere, and to avoid spin-up problems related to unstable surface state, the surface initial conditions of each forecast experiments are obtained from the corresponding surface offline simulations. The focus is on short-range forecasts which have the advantage that the synoptic situation is in the predictable range. Still, changes in albedo and LAI would have an impact on near-surface atmosphere through radiative forcing and sensible and latent

heat flux. Screen-level temperature and moisture can be verified using the analysis, which draws closely to the surface synoptic observations. The model is run with 137 vertical levels at T511 (~40 km) horizontal resolution. The experiments configurations are summarized in Table 1.

The assessment of the NRT impact is done for the screen-level temperature and relative humidity through two metrics named hereafter sensitivity and impact:

$$\text{sensitivity}(T) = T_{\text{exp}} - T_{\text{ctl}} \quad (4)$$

$$\text{impact}(T) = |T_{\text{ctl}} - T_{\text{an}}| - |T_{\text{exp}} - T_{\text{an}}| \quad (5)$$

Where subscripts *ctl* refers to climatological LAI/albedo based forecast, *exp* refers to NRT LAI/albedo based forecast and “*an*” refer to the operational analysis. The equivalent quantities are computed for relative humidity. Therefore a positive (negative) sensitivity would mean an increase (decrease) of temperature/relative humidity at the 2-m level due to assimilation of the NRT data. A positive (negative) impact means a reduction (increase) of the 2-m temperature/relative humidity error in comparison to the operational analysis due to the use of the NRT analysis.

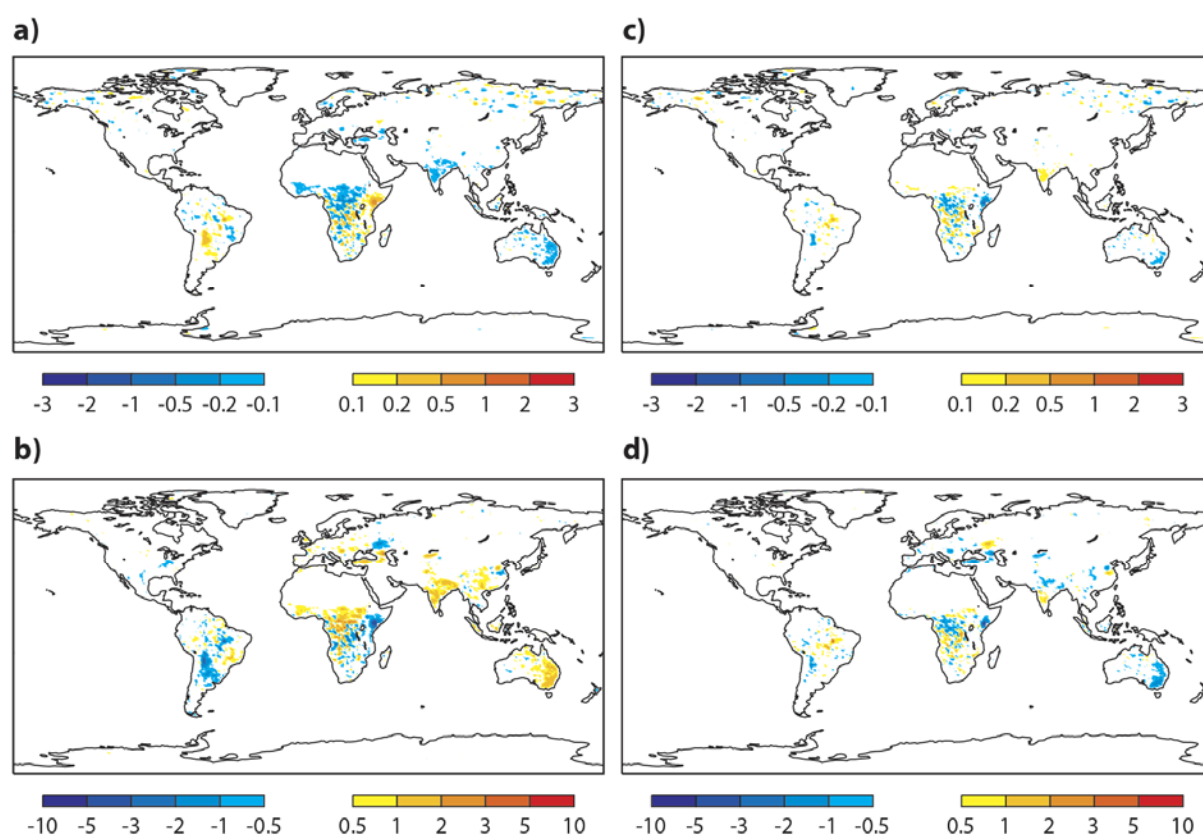


Figure 11: Scores of forecast experiment using LAI NRT (FLAINRT) against experiment using climatology (FCLIM) for November 2010: a) 2-m temperature sensitivity [K], b) 2-m relative humidity sensitivity [%], c) 2-m temperature impact, and d) 2-m relative humidity impact.

Figure 11 shows the results of the forecast experiment using the LAI NRT analysis (FLAINRT) for the global land for the 36-hour forecast (valid at 12 UTC) in comparison to the control run FCLIM related to the use of LAI climatology for November 2010. The use of NRT LAI resulted in a neutral to positive impact for the global 2-m temperature (Figure 11c). In this case, the bias reduction corresponds to a temperature change that reaches 2 K mainly caused by the LAI anomaly, with a warming over the Horn of Africa co-located with the LAI reduction and a cooling co-located with the LAI positive anomaly over eastern Australia (Figure 11a). The African tropics also experienced a cooling partially related to a positive LAI anomaly which contributed in reducing the temperature bias in comparison with the operational analysis. However a similar cooling over the Indian peninsula resulted in a mild bias increase of 0.2 K. The relative humidity results show similar patterns. The regions which have a temperature increase display a drying in the relative humidity, while the regions that have a cooling show a moistening in the relative humidity (Figure 11b). As for the temperature results, the changes in the relative humidity which are co-located with the LAI anomaly correspond in general to a bias reduction in comparison with the operational analysis relative humidity (Figure 11d). In the case of the FNRT forecast experiment where both LAI and albedo NRT analysis are used, the results are quite similar to the FLAINRT experiment where only LAI inter-annual variability is represented through the NRT analysis and albedo is climatology (Figure 12). The only noticeable difference can be seen over central and eastern Australia where the negative albedo anomaly occurred; in this case the cooling/moistening (Figure 11a/b) caused by the LAI positive anomaly was reduced and even reversed compared to FLAINRT (Figures 12a/b). This can be explained by the darkening of the surface albedo (Figure 4c) which caused an increase of the absorbed surface radiation and consequently an increase in the sensible heat flux as depicted in the offline experiment (Figure 9). The positive impact related to this sensitivity is in general preserved (Figure 12c,d) except in central Australia where the warming/drying mildly increased the temperature/relative humidity bias compared to the operational analysis.

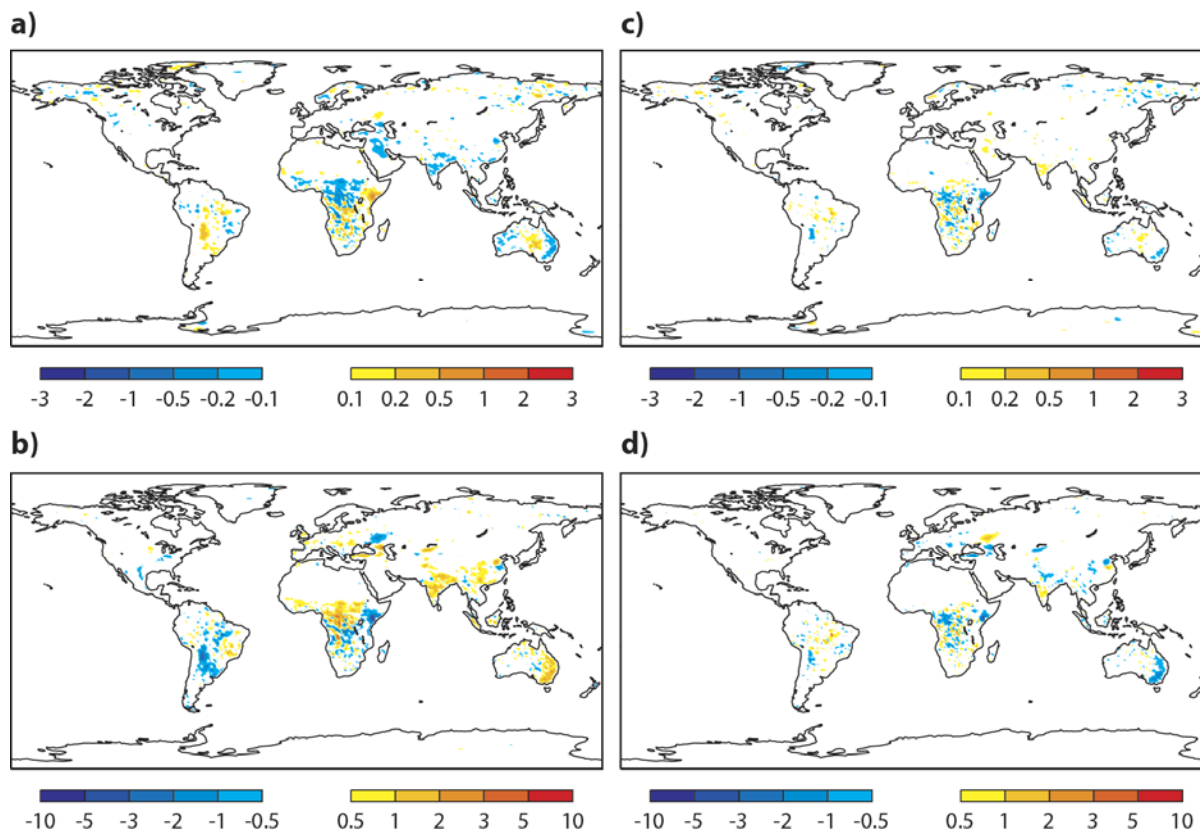


Figure 12: Scores of forecast experiment using LAI and albedo NRT (FNRT) against experiment using climatology (FCLIM) for November 2010: a) 2-m temperature sensitivity [K], b) 2-m relative humidity sensitivity [%], c) 2-m temperature impact, and d) 2-m relative humidity impact.

An additional analysis is performed to investigate a possible link between the precipitation field and the LAI and albedo NRT anomalies. Figure 13 shows the day-3 precipitation (48–72 h) from the forecast experiment using the climatological data (FCLIM) and the differences of the experiments where LAI and albedo are from the NRT analysis with respect to FCLIM. The use of LAI NRT (Figure 13b, c) results in a decrease of the precipitation over the Horn of Africa and a slightly mixed signal with a predominant overall increase over central and eastern Australia. On the other hand, the albedo anomaly, although having a slight impact on the evaporation (Figure 8), was not translated into a precipitation anomaly (Figure 13b, d). The above-mentioned correlation between the LAI and evaporation anomalies and precipitation patterns in some regions suggest that precipitation in those regions is partially driven by evaporation through local surface-atmosphere interaction mechanism. For instance, in the case of the Horn of Africa, Dutra et al. (2013) showed that precipitation in that region is driven by ENSO but also by local surface-atmosphere interaction. However this is not true everywhere; in other regions like central South America the differences in evaporation (Figure 9) are not correlated with the differences in precipitation.

In addition, this precipitation pattern linked to anomalous LAI regions is already established even at the 24-h forecast range. This suggest that precipitation is sensitive to the surface conditions even at the short range and that the initialisation of surface conditions from offline simulations results is effective in overcoming the surface spin-up problem.

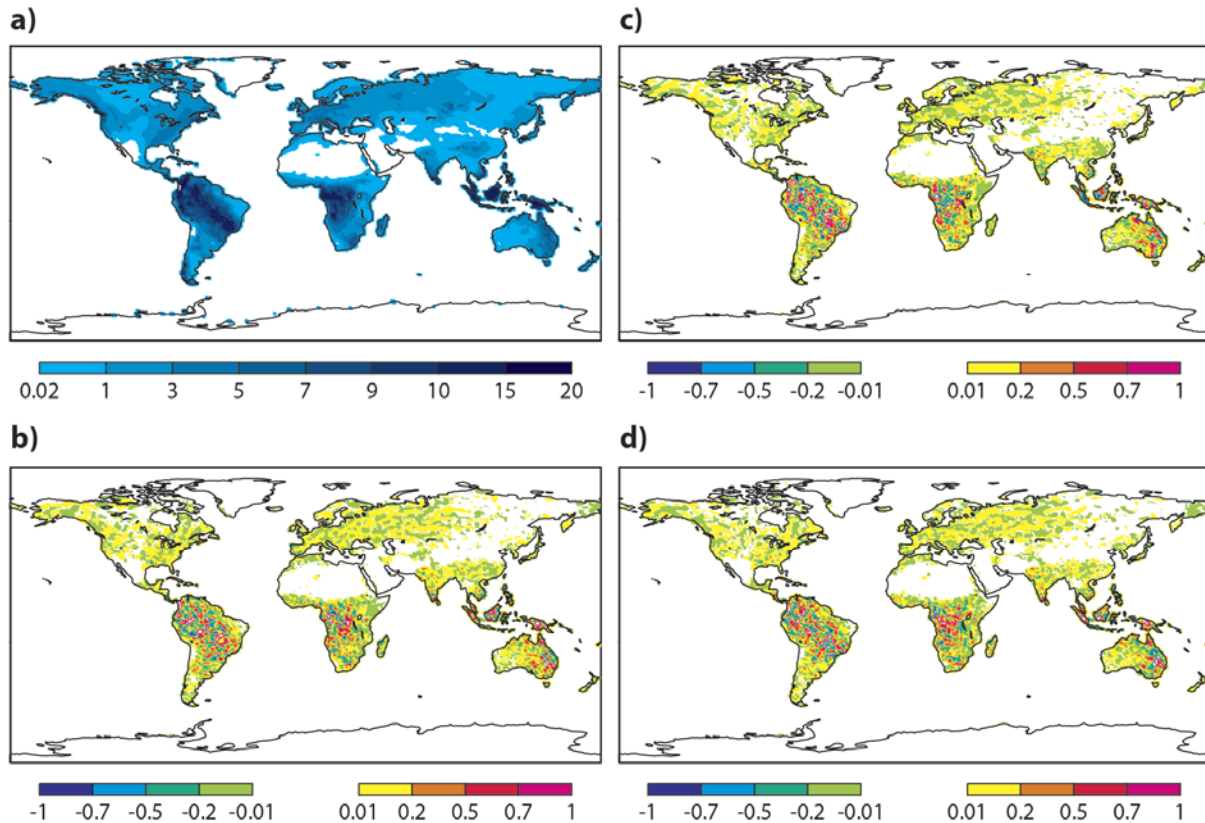


Figure 13: Forecast total precipitation [mm/day] for 48 to 72 hour range using LAI and albedo climatology (a), and difference with simulation using LAI NRT analysis (FLAINRT-FCLIM) (b), difference with simulation using LAI and albedo NRT analysis (FNRT-FCLIM) (c), difference between simulation using LAI NRT analysis and simulation using both LAI and albedo NRT analysis (FNRT-FLAINRT) (d).

4 Conclusions

Owing to the importance of the vegetation in the land–atmosphere interaction processes, numerous studies have tried to use the satellite observations to give information on the vegetation layer, and attempted to evaluate the quality of this information through their signals and impacts. This study proposes an optimal interpolation analysis of the GEOV1 surface albedo and LAI through the combination of the satellite observations and derived climatologies. This assimilation system is able to correct deficiencies in the satellite observation product, especially in high latitudes and snow covered areas as well as in the cloud contaminated areas. The final products have smoother spatial and temporal evolution, which make them more appropriate for environmental and numerical weather

prediction. These assimilated products are also able to detect extreme events where in wet cases the LAI could be well beyond the 90th percentiles and in dry cases it could be below the 10th percentiles of the considered 14 years' time series. This was also the case for the surface albedo but extremes values are in the opposite direction as albedo decreases in wet cases and increases in dry conditions.

Two types of global model experiments (stand-alone surface simulation and medium-range forecasts) were performed to assess the impact of using these NRT analysis products on the surface and near-surface atmosphere. The offline surface runs show that extreme NRT LAI anomalies have a strong impact on the surface energy and CO₂ fluxes, larger than the albedo anomalies which have a smaller range. In addition, an evaluation against in-situ observations showed that a neutral to slightly better fit with in-situ surface soil moisture (from ISMN) and surface energy and CO₂ fluxes (from FLUXNET) can be obtained when using the NRT analysis products although the average signal can be weakened from non-anomalous areas/sites.

The evaluation of using the NRT LAI and albedo analysis in forecast runs shows an overall positive impact on the near-surface temperature and humidity especially in areas where the LAI anomaly is pronounced. In these cases, the near-surface air temperature and humidity errors, both in wet and dry conditions, are reduced. It is also shown that NRT albedo, given its reduced inter-annual variability, has a smaller impact which is mainly seen in wet cases when albedo anomalies are more pronounced. The impact on precipitation fields revealed that in some regions the differences in precipitations fields, evapotranspiration and NRT LAI are correlated. In these regions, the local surface-atmosphere interaction is believed to be one of the important drivers for precipitation, however further investigation supported by additional in-situ observation is needed to confirm such hypothesis.

The offline surface runs and forecasts experiments confirm the benefit coming from a more realistic treatment of vegetation by the use of NRT LAI and albedo analysis. With NRT analysis products, anomalous year could be detected and surface fluxes were directly affected by their inter-annual variability. The forecast simulation confirmed this positive impact on the near-surface weather parameters and its potential to account for NRT issues such as a rapid change in the LAI due to fast growth or harvest as well as inter-annual variability due to an extreme drought or an extensive snow season that may inhibit growth.

However, some caveats on the generality of these results within the ECMWF modelling system are to be mentioned. For instance ad-hoc separations of momentum budget from vegetation cycle are currently adopted (e.g. a constant vegetation roughness length per given vegetation type, Sandu et al. 2013) and may artificially reduce the sensitivity to vegetation state anomalies. Similarly the interaction of albedo, considering broad-band anomalies is less sensitive to vegetation variability than considering only the near infra-red component (Gao et al., 2005). In addition, the treatment of albedo in presence of snow (using a climatological vegetation albedo per given type, Dutra et al. 2010) reduces the impact

of albedo anomalies for early/late senescence or greening. These effects discussed above, related to LAI and albedo treatment in the modelling system, are going towards a reduction of atmospheric impact. Therefore an update of the system to take into account these processes would reinforce the influence of the vegetation and albedo on weather prediction.

Acknowledgements:

We thank Peter Bechtold, Patricia de Rosnay, Roselyne Lacaze and Jean Christophe Calvet for their support and fruitful comments on the results, Anabel Bowen for her help on the figures improvements and Bob Riddaway for his careful review and improvements of the use of the English language. This work used eddy covariance data acquired by the FLUXNET community and in particular by the following networks: AmeriFlux (U.S. Department of Energy), Biological and Environmental Research, Terrestrial Carbon Program (DE-FG02-04ER63917 and DE-FG02-04ER63911), CarboItaly, CarboMont, Fluxnet-Canada (supported by The Canadian Foundation for Climate and Atmospheric Sciences (CFCAS), The Natural Sciences and Engineering Research Council of Canada (NSERC), BIOCAP Foundation, Environment Canada, and Natural Resources Canada (NRCan)), the Sources and Sinks of Greenhouse Gases from managed European Grasslands and Mitigation Strategies (GreenGrass) project, the Large-scale Biosphere-Atmosphere Experiment in Amazonia (LBA), the Nordic Centre for Studies of Ecosystem carbon exchange and its Interaction with the Climate system (NECC), the Terrestrial Carbon Observation System Siberia (TCOS-Siberia). We thank in particular the PIs that decided to share their data freely within the scientific community. We acknowledge the support to the eddy covariance data harmonization provided by the Integrated Project Assessment of the European Terrestrial Carbon Balance (CarboEuropeIP), The Food and Agriculture Organization-The Global Terrestrial Observing System-The Terrestrial Carbon Observations project (FAO-GTOS-TCO), the Integrated Land Ecosystem-Atmosphere Processes Study (iLEAPS), Max Planck Institute for Biogeochemistry, National Science Foundation, University of Tuscia, Université Laval and Environment Canada and US Department of Energy and the database development and technical support from Berkeley Water Center, Lawrence Berkeley National Laboratory, Microsoft Research eScience, Oak Ridge National Laboratory, University of California - Berkeley, University of Virginia. We also thank The Fluxnet-Canada Research Network for making available the BERMS data (<http://berms.ccrp.ec.gc.ca/Overview/e-overview-about.htm>), the PIs and researchers involved in the Coordinated Enhanced Observing Period (CEOP) project for provision and archiving of the data used in this study (<http://www.ceop.net/>), and the CARBOSCOPE project contributors for making their data freely available through the project website (<http://www.carboscope.eu/?q=home>). We thank also all the PIs of the International Soil Moisture Network (ISMN) that decided to share their data freely within the scientific community (<https://ismn.geo.tuwien.ac.at/ismn/>). We further thank Bruno

Smets from VITO for his support on the GEOV data provision (<http://land.copernicus.eu/global/>). This work is a contribution to the ImagineS project (<http://fp7-imagines.eu/>), funded by the European Commission 7th Framework Programme in support to the Copernicus Global land.

References

- Avissar, R., & Liu, Y. (1996). Three-dimensional numerical study of shallow convective clouds and precipitation induced by land surface forcing. *J. of Geophys. Res.*, 101, 7499–7518.
- Baldocchi, D., et al., (2001). FLUXNET: A new tool to study the temporal and spatial variability of ecosystem-scale carbon dioxide, water vapor, and energy flux densities. *Bull. Am. Meteorol. Soc.*, 82, 2415-2434, doi:10.1175/1520-0477.
- Baldocchi D., (2008). Breathing of the terrestrial biosphere: lessons learned from a global network of carbon dioxide flux measurement systems. *Aust. J. Bot.*, 56, 1–26.
- Balsamo, G., Viterbo, P., Beljaars, A., van den Hurk, B., Hirschi, M., Betts, A. K., & Scipal, K. (2009). A Revised Hydrology for the ECMWF Model: Verification from Field Site to Terrestrial Water Storage and Impact in the Integrated Forecast System. *J. Hydrometeorol.*, 10, 623-643.
- Balsamo, G., Boussetta, S., Dutra, E., Beljaars, A., Viterbo, P. & Van den Hurk, B. (2011). Evolution of land surface processes in the IFS, *ECMWF Newsletter*, 127, 17-22.
- Baret, F., Weiss, M., Lacaze, R., Camacho, F., Makhmara, H., Pacholczyk, P., et al., (2013). GEOV1: LAI and FAPAR essential climate variables and FCOVER global time series capitalizing over existing products. Part1: Principles of development and production. *Rem. Sens. Envir.*, 137, 299–309, <http://dx.doi.org/10.1016/j.rse.2012.12.027>.
- Baret, F., Hagolle, O., Geiger, B., Bicheron, P., Miras, B., Huc, M., Berthelot, B., Niño, F., Weiss, M., Samain, O., Roujean, J. L., & Leroy, M. (2007). LAI, fAPAR and fCover CYCLOPES global products derived from VEGETATION. Part 1: Principles of the algorithm. *Rem. Sens. Envir.*, 110, 530 275–286.
- Beljaars, A., Viterbo, P., Miller, M., & Betts, A. K. (1996). The anomalous rainfall over the United States during July 1993: Sensitivity to land surface parameterization and soil moisture anomalies, *Mon. Weather Rev.*, 124, 362–383.
- Bell, J. E., Palecki, M. A., Baker, C. B., Collins, W. G., Lawrimore, J. H., Leeper, R. D., Hall, M. E., Kochendorfer, J., Meyers, T. P., Wilson, T. & Diamond, H. J. (2013). U.S. Climate Reference Network soil moisture and temperature observations. *J. Hydrometeorol.*, 14, 977-988. doi: 10.1175/JHM-D-12-0146.1, 2013.

- Berbet, M. L. C. & Costa, M. H. (2003). Climate Change after Tropical Deforestation: Seasonal Variability of Surface Albedo and Its Effects on Precipitation Change. *J. Climate*, 16, 2099–2104. doi: [http://dx.doi.org/10.1175/1520-0442\(2003\)016<2099:CCATDS>2.0.CO;2](http://dx.doi.org/10.1175/1520-0442(2003)016<2099:CCATDS>2.0.CO;2)
- Betts, A.K., Ball, J.H., Beljaars, A., Miller, M., & Viterbo, P., (1996). The land-surface-atmosphere interaction: A review based on observational and global modelling perspective. *J. Geophys. Res.*, 101, 7209-7225.
- Betts, A.K., Ball, J.H., Barr, A. G., Black, T. A., McCaughey, J. H. & Viterbo, P. (2006). Assessing land-surface-atmosphere coupling in the ERA-40 re-analysis with boreal forest data. *Agric. For. Meteorol.*, 140, 355-382.
- Boussetta, S., Koike, T., Kun, Y., Graf, T. & Pathmathevan, M. (2008). Development of a coupled land-atmosphere satellite data assimilation system for improved local atmospheric simulations. *Rem. Sens. Envir.*, 112, 720-734.
- Boussetta, S., Balsamo, G., Beljaars, A., Kral, T. & Jarlan, L. (2013a). Impact of a satellite-derived Leaf Area Index monthly climatology in a global Numerical Weather Prediction model, *Int. J. Rem. Sens.*, 34 (9-10), 3520-3542.
- Boussetta, S. et al., (2013b). Natural land carbon dioxide exchanges in the ECMWF Integrated Forecasting System: Implementation and Offline validation. *J. Geophys. Res.* 118, 1-24. doi:10.1002/jgrd.50488.
- Camacho, F., Cernicharo, J., Lacaze, R., Baret, F. & Weiss, M. (2013). GEOV1: LAI, FAPAR Essential Climate Variables and FCOVER global time series capitalizing over existing products. Part 2: Validation and intercomparison with reference products. *Rem. Sens. Envir.* 137, 310–329, <http://dx.doi.org/10.1016/j.rse.2013.02.030>.
- Deardorff, J.W., (1978). Efficient prediction of ground surface temperature and moisture, with inclusion of a layer of vegetation. *J. Geophys. Res.*, **83**, 1889-1903.
- Dee, D. P., et al., (2011). The ERA-Interim reanalysis: Configuration and performance of the data assimilation system, *Q. J. R. Meteorol. Soc.*, doi: 10.1002/qj.828.
- Dorigo, W. A., Wagner, W., Hohensinn, R., Hahn, S., Paulik, C., Xaver, A., Gruber, A., Drusch, M., Mecklenburg, S., van Oevelen, P., Robock, A., & Jackson, T. (2011). The International Soil Moisture Network: a data hosting facility for global in situ soil moisture measurements, *Hydrol. Earth Syst. Sci.*, 15, 1675-1698, doi:10.5194/hess-15-1675-2011.
- Dorman, J.L. & Sellers, P. J. (1989). A Global Climatology of Albedo, Roughness Length and Stomatal Resistance for Atmospheric General Circulation Models as Represented by the Simple Biosphere Model (SiB). *J. Appl. Meteorol.*, 28, 833-855.

- Dutra, E., Balsamo, G., Viterbo, P., Miranda, P.M.A., Beljaars, A., Schär, C., Elder, K., (2010). An improved snow scheme for the ECMWF land surface model: description and offline validation. *J. Hydrometeor.* 11, 899-916. doi: 10.1175/2010JHM1249.1.
- Dutra, E., Magnusson, L., Wetterhall, F., Cloke, H. L., Balsamo, G., Boussetta, S. & Pappenberger, F. (2013). The 2010–2011 drought in the Horn of Africa in ECMWF reanalysis and seasonal forecast products. *Int. J. Climatol.*, 33, 1720–1729. doi: 10.1002/joc.3545.
- Fang, H., Wei, S., & Liang, S. (2012). Validation of MODIS and CYCLOPES LAI products using global field measurement data. *Rem. Sens. Envir.*, 119, 43–54. doi:10.1016/j.rse.2011.12.006.
- Fang, H., et al. (2013). Characterization and intercomparison of global moderate resolution leaf area index (LAI) products: Analysis of climatologies and theoretical uncertainties, *J. Geophys. Res. Biogeosci.*, 118, 529–548, doi:10.1002/jgrg.20051.
- Gao, F., Schaaf, C., Strahler, A., Roesch, A., Lucht, W., & Dickinson, R. (2005). The MODIS BRDF/Albedo Climate Modeling Grid Products and the Variability of Albedo for Major Global Vegetation Types, *J. Geophys. Res.*, 110, D01104, doi:10.1029/2004JD00519.
- Garrigues S., Lacaze, R., Baret, F., Morisette, J. T., Weiss, M., Nickeson, J. E., Fernandes, R., Plummer, S., Shabanov, N. V., Myneni, R. B., Knyazikhin, Y., & Yang, W. (2008). Validation and intercomparison of global Leaf Area Index products derived from remote sensing data. *J. Geophys. Res.*, 113, G02028, doi:10.1029/2007JG000635.
- Geiger, B. & Samain, O. (2004). Albedo determination, Algorithm Theoretical Basis Document, of the CYCLOPES project, version 2.0, 25p. Météo-France/CNRM.
- Giard, D. & Bazile, E. (2000). Implementation of a new assimilation scheme for soil and surface variables in a Global NWP model. *Mon. Weath. Rev.*, 128, 997-1015.
- Guillevic, P., Koster, R. D., Suarez, M. J., Bounoua, L., Collatz, G. J., Los, S. O., & Mahanama, S.P.P. (2002). Influence of the interannual variability of vegetation on the surface energy balance - a global sensitivity study. *J. Hydrometeor.*, 3, 617-629.
- Hagolle, O., Lobo, A., Maisongrande, P., Cabot, F., Duchemin, B., de Pereyra, A. (2004). Quality assessment and improvement of temporally composited products of remotely sensed imagery by combination of VEGETATION 1 and 2 images. *Rem. Sens. Envir.*, 94, 172-186.
- Kallberg, P., (2011), Forecast drift in ERA-Interim, ERA report series, No **10**, http://www.ecmwf.int/publications/library/ecpublications/_pdf/era/era_report_series/RS_10.pdf
- Knote, C., Bonafe, G., & Di Giuseppe, F. (2009). Leaf Area Index Specification for Use in Mesoscale Weather Prediction Systems. *Mon. Weath. Rev.*, 137, 3535-3550.

- Koster, R. D., Mahanama, S., Yamada, T., Balsamo, G., Boisserie, M., et al., (2010). The Contribution of Land Surface Initialization to Subseasonal Forecast Skill: First Results from the GLACE-2 Project, *Geophys. Res. Lett.*, 37, L02402, doi:10.1029/2009GL041677.
- Lawrence, D. M. & Slingo, J. M. (2004). An annual cycle of vegetation in a GCM. Part I: implementation and impact on evaporation, *Clim. Dynam.*, 22, 87-105.
- Loveland, T. R., Reed, B. C., Brown, J. F., Ohlen, D. O., Zhu, Z., Youing, L., & Merchant, J. W. (2000). Development of a global land cover characteristics database and IGB6 DISCover from the 1km AVHRR data. *Int. J. Rem. Sens.*, 21, 1303–1330.
- Myneni, R. B., Hoffman, S., Knyazikhin, Y., Privette, J. L., Glassy, J., Tian, Y., Wang, Y., Song, X., Zhang, Y., Smith, G. R., Lotsch, A., Friedl, M., Morisette, J. T., Votava, P., Nemani, R. R., Running, S. W. (2002). Global products of vegetation leaf area and fraction absorbed PAR from year one of MODIS data. *Rem. Sens. Envir.*, 83, 214-231.
- Pielke, R. A., & Avissar, R. (1990). Influence of landscape structure on local and regional climate, *Landscape Ecol.*, 4, 133–155, doi:10.1007/BF00132857.
- Preuss, H. J., & Geleyn, J. F. (1980). Surface albedos derived from satellite data and their impact on forecast models, *Meteorol. Atmos. Phys.*, 29A, 345–356, doi:10.1007/BF02245431.
- Rahman, H. & Dedieu, G. (1994). SMAC: a simplified method for the atmospheric correction of satellite measurements in the solar spectrum. *Int. J. Rem. Sens.*, 15(1): 123-143.
- Roujean, J.-L., Leroy, M. & Deschamps, P.-Y. (1992). A bidirectional reflectance model of the Earth's surface for the correction of remote sensing data. *J. Geophys. Res.*, 97(D18), 20455-20468.
- Rowell D. P., & Blondin, C. (1990), The influence of soil wetness distribution on short-range rainfall forecasting in the West African Sahel. *Q. J. R. Meteorol. Soc.*, 116, 496, 1471–1485. DOI: 10.1002/qj.49711649611.
- Sandu, I., Beljaars A., Bechtold P., Mauritsen T. & Balsamo G. (2013), Why is it so difficult to represent stably stratified conditions in numerical weather prediction (NWP) models?, *J. Adv. Model. Earth Syst.*, 5, 117–133, doi:10.1002/jame.20013.
- Sellers, P.J., Los, S. O., Tucker, C. J., Justice, C. O., Dazlich, D. A., Collatz, G. J. & Randall, D. A., (1996). A revised land surface parameterization (SiB2) for atmospheric GCMs, Part II: The generation of global fields of terrestrial biophysical parameters from satellite data. *J. Clim.*, 9, 676–705.
- Van den Hurk, B., Viterbo, P., & Los, S. (2003a). Impact of leaf area index seasonality on the annual land surface evaporation in a global circulation model. *J. Geophys. Res.*, 108, D6, 4191, doi:10.1029/2002JD002846.

- Van den Hurk, B. & Viterbo, P. (2003b). The Torne-Kalix PILPS 2(e) experiment as a test bed for modifications to the ECMWF land surface scheme. *Global and Planetary Change*, 38, 165–173.
- Verger, A., Baret, F., Weiss, M. (2011). A multisensor fusion approach to improve LAI time series. *Rem. Sens. Enviro.*, DOI: 10.1016/j.rse.2011.05.
- Viterbo, P. & Beljaars, A. (1995). An improved land surface parametrization scheme in the ECMWF model and its validation, *ECMWF Technical Report*, 75, Reading, UK.
- Viterbo P., Beljaars, A., Mahouf, J.-F., Teixeira, J. (1999). The representation of soil moisture freezing and its impact on the stable boundary layer. *Q. J. R. Meteorol. Soc.* 125, 2401–2426.
- Xue, Y., Fennessy, M.J. & Sellers, P.J. (1996). Impact of vegetation properties on U.S. Summer weather prediction. *J. Geophys. Res.*, 101D, 7419-7430.